Proceedings of the Institution of Civil Engineers
**Geotechnical Engineering 149**
October 2001 Issue 4
Pages 1–14

**Paper 13008**

Received 00/00/0000
Accepted 00/00/0000

**Keywords:** geotechnical engineering/mathematical modelling/strength & testing of materials

**N. Al-Shayea**
Associate Professor, Department of Civil Engineering, King Fahd University of Petroleum & Minerals, Saudi Arabia

**S. Abduljauwad**
Professor, Department of Civil Engineering, King Fahd University of Petroleum & Minerals, Saudi Arabia

**R. Bashir**
Research Assistant, Department of Civil Engineering, King Fahd University of Petroleum & Minerals, Saudi Arabia

**H. Al-Ghamedy**
Associate Professor, Department of Civil Engineering, King Fahd University of Petroleum & Minerals, Saudi Arabia

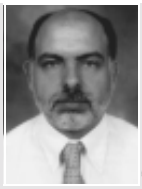

**I. Asi**
Associate Professor, Department of Civil Engineering, King Fahd University of Petroleum & Minerals, Saudi Arabia

# Determination of parameters for a hyperbolic model of soils from the eastern province of Saudi Arabia

N. Al-Shayea, S. Abduljauwad, R. Bashir, H. Al-Ghamedy and I. Asi

**Analysis of some geotechnical problems using finite element methods requires the implementation of a non-linear model for soil materials, to better represent their actual behaviour. Constitutive modelling of soil mass behaviour and material interfaces is an essential component of the solution of boundary and initial value problems. The hyperbolic model is one of the most frequently used non-linear models for predicting the behaviour of soils in boundary value problems. The parameters of this model for specific soils need to be determined experimentally. This paper presents the results of extensive laboratory testing carried out on three soils from the Eastern Province of Saudi Arabia: sand, marl, and sabkha. The tests used to obtain these results were the triaxial compression test, the hydrostatic (isotropic compression) test, and the direct shear test. Additionally, other tests were used to obtain various physical properties needed for the complete characterisation of these soils. Parameters of the hyperbolic models for non-linear tangent Young's and bulk moduli are presented. These parameters compare well with those reported in the literature. They are incorporated in the hyperbolic model and used to back-predict the stress–strain behaviour of the investigated soils. The calibrated models are found to predict soil behaviour very well.**

## NOTATION

| | |
|---|---|
| $B$ | bulk modulus |
| $B_i$ | initial tangent bulk modulus |
| $B_t$ | tangent bulk modulus |
| $C$ | cohesion |
| $C_c$ | coefficient of curvature |
| $C_u$ | coefficient of uniformity |
| $D_r$ | relative density |
| $E_i$ | initial tangent Young's modulus |
| $E_t$ | tangent Young's modulus |
| $G_s$ | specific gravity |
| $K$ | hyperbolic parameter 1 for Young's modulus |
| $n$ | hyperbolic parameter 2 for Young's modulus |
| $P_a$ | atmospheric pressure |
| RC | relative compaction |
| $R_f$ | failure ratio |
| $w$ | water content |
| $w_n$ | natural water content |
| $w_{opt}$ | optimum water content |
| $\Delta H$ | horizontal displacement |
| $\Delta\varepsilon_{vol}$ | change in volumetric strain |
| $\Delta\sigma_m$ | change in mean stress |
| $\Delta\phi$ | reduction in angle of internal friction between $\sigma_3 = P_a$ and $\sigma_3 = 10P_a$ |
| $\varepsilon$ | axial strain |
| $\varepsilon_u$ | ultimate volumetric strain at large stress |
| $\varepsilon_{vol}$ | volumetric strain |
| $\rho_d$ | dry density |
| $\rho_{d,max}$ | maximum dry density |
| $\rho_{field}$ | field density |
| $\rho_{min}$ | minimum density |
| $\rho_{max}$ | maximum density |
| $\sigma$ | normal stress on failure plane |
| $\sigma_m$ | mean stress (confining pressure for hydrostatic load) |
| $\sigma_n$ | normal stress |
| $\sigma_1$ | major principal stress |
| $\sigma_3$ | minor principal stress, confining pressure (in triaxial test) |
| $\sigma_1 - \sigma_3$ | deviator stress |
| $(\sigma_1 - \sigma_3)_f$ | actual deviator stress at failure |
| $(\sigma_1 - \sigma_3)_u$ | ultimate deviator stress at large strain (theoretical) |
| $\tau$ | shear strength of soil |
| $\tau$ | shear stress |
| $\phi$ | angle of internal friction |
| $\phi_o$ | angle of internal friction at $\sigma_3 = P_a$ |

## 1. INTRODUCTION

Soils are very complicated engineering materials, whose constitutive response depends on many compositional and environmental factors. The problem manifests itself in the non-linear deformation of soil under mechanical loads. The availability of high-speed computers and powerful numerical techniques (such as the finite element method) makes it possible to incorporate the non-linear behaviour of materials into the analysis of soil systems and soil–structure interaction problems. Some advanced soil models have been proposed for the non-linear stress–strain behaviour of soils, including the hypoelastic models,[1] the hyperelastic models,[2,3] and the



Article number = 13008

plasticity models.[4] However, these models require the determination of many parameters for the investigated soils.

Non-linear elastic or piecewise linear elastic models have been developed to account for the influence of stress or strain on material behaviour. These include models based on the functional representation of one or more observed stress–strain and volumetric response curves. Hyperbolic representation has been used for static and quasi-static behaviour, and can provide a satisfactory prediction of load–displacement behaviour under monotonic loading.[5]

In this paper, the hyperbolic model was employed for simulating the stress–strain response of soils, which is needed for the analysis and design of important geotechnical projects. The theoretical background of such a model is presented. Three soil types were used in this investigation, and they have been thoroughly characterised. Parameters for the hyperbolic model were determined experimentally for these local soils from the Eastern Province of Saudi Arabia.

## 2. BACKGROUND

A brief overview of the hyperbolic model for soil is presented. In this work, emphasis was placed on the parameters of the model and their determination, from laboratory characterisation of representative soil samples. The hyperbolic model is a variable-parameter model used to simulate the non-linear stress–strain response of soils, and is often used with numerical solution techniques such as the finite element method.[4,6] The use of hyperbolae was proposed to represent the stress–strain behaviour of cohesive soils[7] and cohesionless soils.[8] The model was modified by Hansen.[9] Since the stress–strain behaviour of soil depends on confining stress, Duncan and Chang[5] incorporated that effect and used the hyperbola in conjunction with the relationship between the initial modulus and confining pressure proposed by Janbu.[10]

Duncan and Chang[5] and Duncan *et al.*[11] presented a non-linear stress–strain model based on a hyperbolic type of relation between the deviator stress ($\sigma_1 - \sigma_3$) and the axial strain ($\varepsilon$), which is determined from triaxial test results. This model is defined by a variable Young's modulus and a variable bulk modulus. Young's modulus increases with increasing confining stress and decreases with increasing shear stress. The bulk modulus also increases with confining pressure, and is related to the power of the confining stress. The model uses isotropic linear-elastic stress–strain relationships but with the elastic parameters varied according to the stress state. A tangent, rather than secant, formulation is used for Young's modulus, making this model particularly suitable for incremental simulation.

Selig[12] extended the above model of Duncan *et al.*[11] by using the same Young's modulus formulation but with an alternative bulk modulus having a hyperbolic formulation—that is, a tangent bulk modulus—which is a function of the mean normal stress state. It was found to represent hydrostatic compression better than the power law form proposed by Duncan and Chang.[5] The hyperbolic form was also found capable of representing uniaxial (unconfined) and triaxial compression.

### 2.1. Young's modulus

A typical stress–strain relationship from a constant confining pressure triaxial compression test is shown by the dashed curve in Fig. 1. This relationship is assumed to be represented mathematically by a hyperbola (solid curve, Fig. 1) having the form

$$\sigma_1 - \sigma_3 = \frac{\varepsilon}{\dfrac{1}{E_\mathrm{i}} + \dfrac{\varepsilon}{(\sigma_1 - \sigma_3)_\mathrm{u}}} \qquad (1)$$

where $\varepsilon$ is the axial strain, $E_\mathrm{i}$ is the initial tangent modulus, $(\sigma_1 - \sigma_3)_\mathrm{u}$ is the ultimate deviator stress at large strain, and $\sigma_1$ and $\sigma_3$ are the major and minor principal stresses respectively.

The hyperbola is considered valid up to the actual soil failure (point A). Thus the ultimate deviator stress is defined in terms of the actual failure deviator stress, $(\sigma_1 - \sigma_3)_\mathrm{f}$, by the failure ratio, $R_\mathrm{f}$, as

$$R_\mathrm{f} = \frac{(\sigma_1 - \sigma_3)_\mathrm{f}}{(\sigma_1 - \sigma_3)_\mathrm{u}} \qquad (2)$$

The parameters $E_i$ and $(\sigma_1 - \sigma_3)_u$ can be found by plotting the actual test data in a linearised hyperbolic form. The appropriate straight line used to represent the transformed equation (1) is

$$\frac{\varepsilon}{\sigma_1 - \sigma_3} = \frac{1}{E_\mathrm{i}} + \frac{\varepsilon}{(\sigma_1 - \sigma_3)_\mathrm{u}} \qquad (3)$$

According to Janbu,[10] the initial tangent modulus is assumed to increase with the confining pressure, $\sigma_3$, as follows:

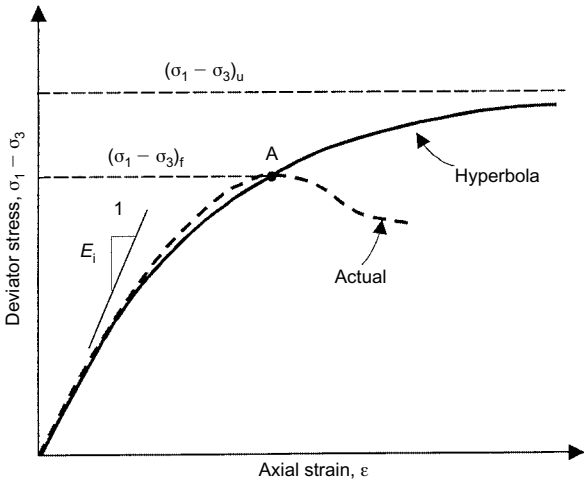


Fig. 1. Comparison of typical stress–strain curve with hyperbola

$$E_i = KP_a(\sigma_3/P_a)^n \quad (4)$$

where $P_a$ is the atmospheric pressure ($P_a = 101{\cdot}325$ kPa), which is used to non-dimensionalise the parameters $K$ and $n$. The parameters $K$ and $n$ can be determined from a logarithmic plot of $E_i/P_a$ against $\sigma_3/P_a$. Because specimens in the present study were drained and not saturated, the stress $\sigma_3$ can be taken as total or effective.

The failure deviator stress is a function of the confining stress, $\sigma_3$. The Mohr–Coulomb failure envelope is represented for simplicity by a straight line with a slope $\phi$ and an intercept $C$. The failure envelope is expressed mathematically by

$$(\sigma_1 - \sigma_3)_f = \frac{2C\cos\phi + 2\sigma_3\sin\phi}{1 - \sin\phi} \quad (5)$$

where $C$ is the cohesion of the soil, and $\phi$ is the angle of internal friction.

The actual envelope is often curved. Thus either the best-fit straight line can be used, or $\phi$ may be varied with $\sigma_3$. The latter case was used in this investigation, and $\phi$ is represented by

$$\phi = \phi_o - \Delta\phi\log_{10}(\sigma_3/P_a) \quad (6)$$

where $\phi_o$ is the value of $\phi$ for $\sigma_3 = P_a$, and $\Delta\phi$ is the reduction in $\phi$ for a tenfold increase in $\sigma_3$.

The tangent Young's modulus for any stress state may be determined by differentiating equation (1), and then using equations (2), (4) and (5). The resulting equation for the tangent modulus is

$$E_t = \left[1 - \frac{R_f(1-\sin\phi)(\sigma_1 - \sigma_3)}{2C\cos\phi + 2\sigma_3\sin\phi}\right]^2 KP_a(\sigma_3/P_a)^n \quad (7)$$

where $\phi$ is as expressed in equation (6).

### 2.2. Bulk modulus

The bulk modulus, $B$, is defined as

$$B = \frac{\Delta\sigma_m}{\Delta\varepsilon_{vol}} \quad (8)$$

where $\Delta\sigma_m$ is the change in mean stress, and $\Delta\varepsilon_{vol}$ is the change in volumetric strain.

Duncan *et al.*[11] proposed a formulation for $B$ based on data from triaxial tests. An alternative method for obtaining the bulk modulus is from a hydrostatic (isotropic) compression test. In this test, the soil specimen is compressed under an increasing confining pressure applied equally in all directions. According to equation (8), the tangent bulk modulus, $B_t$, is the slope of the hydrostatic stress–strain curve. Selig[12] observed that the curve relating hydrostatic confining pressure, $\sigma_m$, and the volumetric strain, $\varepsilon_{vol}$, can be reasonably represented by the hyperbolic equation

$$\sigma_m = \frac{B_i\varepsilon_{vol}}{1 - (\varepsilon_{vol}/\varepsilon_u)} \quad (9)$$

where $B_i$ is the initial tangent bulk modulus, and $\varepsilon_u$ is the ultimate volumetric strain at large stress.

The tangent bulk modulus, $B_t$, is determined by differentiating equation (9) and substituting $\varepsilon_{vol}$ also from equation (9). The result is Selig's bulk modulus expression:

$$B_t = B_i\left[1 + \frac{\sigma_m}{B_i\varepsilon_u}\right]^2 \quad (10)$$

To determine the parameters $B_i$ and $\varepsilon_u$, the hydrostatic test data are plotted in a linearised hyperbolic form. Yang[13] and Lin[14] have shown that the hyperbolic formulation for the tangent bulk modulus, equation (10), represents soil behaviour in a hydrostatic compression test better than the formulation proposed by Duncan *et al.*[11]

## 3. GEOLOGY OF THE AREA

The geology of the Arabian Peninsula broadly consists of the Arabian shield in the west and the Arabian shelf in the east. The Arabian shelf comprises a sedimentary succession of Cambrian to Pliocene layers covering the eastern and northern part of the peninsula. In eastern Saudi Arabia, the strata dip gently east and north-east, reflecting the buried basement configuration. The surface rocks of the Eastern Province of Saudi Arabia include formations of consolidated sediments ranging from the Palaeocene to the Middle Eocene and the Miocene to the Pliocene.[15] Unconsolidated materials include various sediments of Quaternary age, comprising wind-blown sand dunes, beach sand and gravel, basin deposits of gravel and silt, sabkha sediments, shale, marl and claystone.[16,17] The generalised geological map of the Eastern Province region is shown in Fig. 2. Recent studies have focused on the geotechnical properties of various geological deposits in the area. Abduljauwad and Al-Amoudi[18] studied the behaviour of saline sabkha soils. Azam *et al.*[19] investigated the expansive characteristics of gypsiferous/anhydritic soil formations. Abduljauwad *et al.*[20] performed laboratory and field measurements to study the response of structures to the heave of expansive clay. Al-Shayea[21] presented a case study of the inherent heterogeneity of sediments in the area.

## 4. SITE SELECTION FOR SOIL MATERIALS

Because this research was supported by the pipeline industry, sampling sites were selected in areas where a pipeline network encountered a specific soil type in the Eastern Province of Saudi Arabia. Emphasis was placed on the surface geology of the area to determine the types of natural soil associated with local pipeline networks, by combining geological maps with pipeline network maps. Three different types of soil were considered: sand, marl, and sabkha. The geological distributions of these soils in the area have been studied by

PROOFS

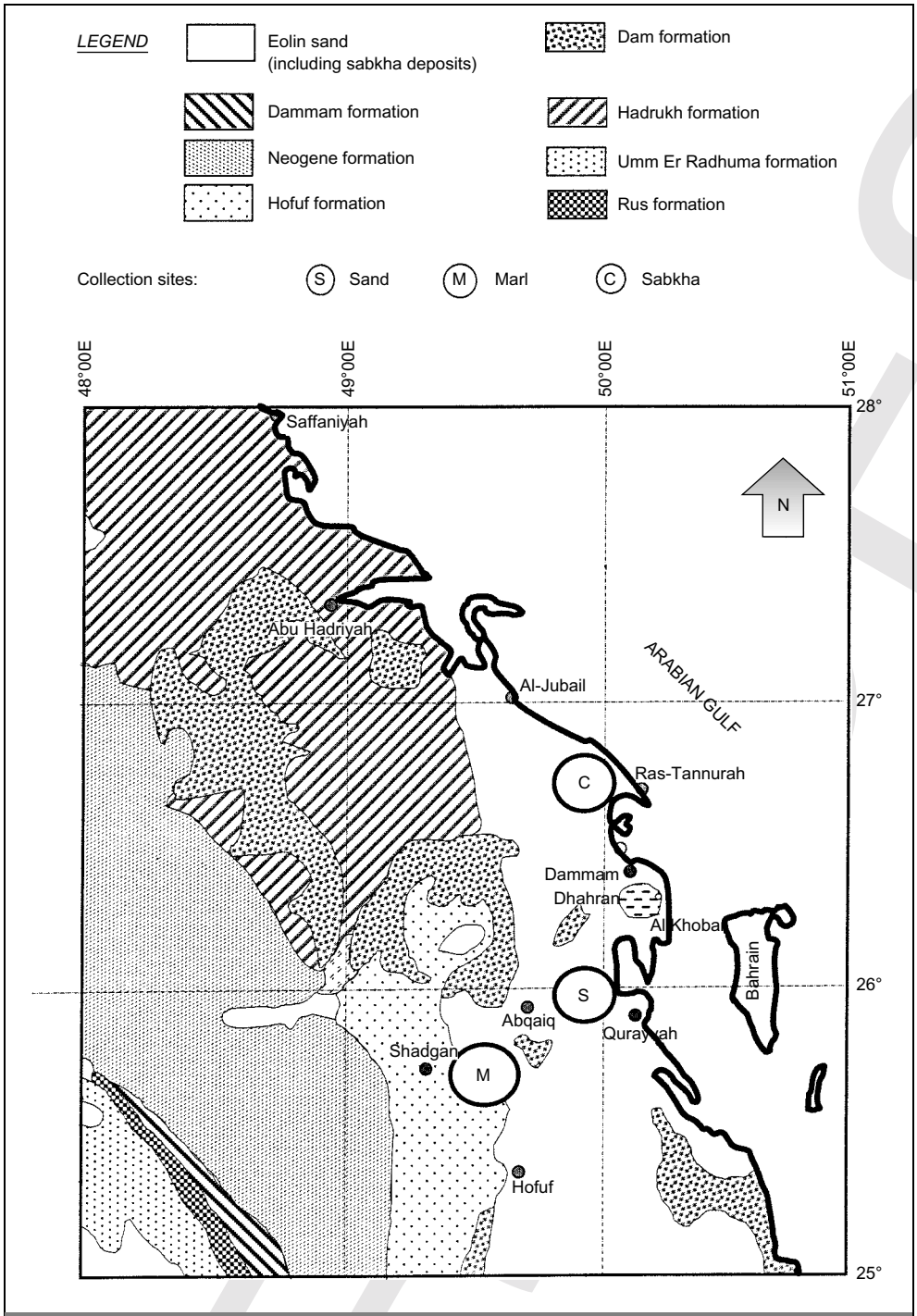


Fig. 2. Geological map of the Eastern Province of Saudi Arabia, with collection sites for soil samples shown

different investigators. Ahmad[22] presented a map showing locations of marl, Al-Ayedi[23] presented a similar map for sabkha, and Al-Gunaiyan[24] presented a similar map for the main sand dune areas. These geological maps were combined with the local pipeline networks in the area to help determine the appropriate sites for collecting samples of different types of soil.

The sand samples were collected from a sand dune close to a pipeline between Al-Qurrayah and Abqaiq. The marl samples were collected from a pipeline trench close to the Shedgum power plant. The sabkha samples were collected from a site beside a pipeline in the Ras Tanurah area. Sampling locations are shown in Fig. 2. The in-situ density of the dune sand was measured in the field using a nuclear gauge, at depths of 5, 10, 20 and 30 cm below the ground surface. Extensive laboratory testing took place in order to characterise all three different soil materials.

## 5. EXPERIMENTAL PROGRAMME

### 5.1. Physical properties

Basic soil properties were determined for the three different soil types. These include the following:

(*a*) Determination of the particle size distribution for the sand and marl soils using sieve analysis, according to ASTM Standards D 421 and D 422.[25] The particle size distribution of the sabkha soil was found using a combination of sieve analysis and the hydrometer method. The washed sieving method was used.
(*b*) Determination of the specific gravity ($G_s$) for all soil types, according to ASTM Standard D 854.
(*c*) Determination of the maximum and minimum density (relative density) for the sand, according to ASTM Standards D 4253 and D 4254.
(*d*) Determination of the moisture–density relationships for the marl and sabkha soils, according to ASTM Standard D 1557 (modified Proctor test).
(*e*) Determination of the natural water content and Atterberg limits (liquid limit and plastic limit) for the sabkha soil, according to ASTM D 2216 and D 4318 respectively.

### 5.2. Mechanical properties

The mechanical properties of the three soil types were determined at two different conditions (loose and dense). The sand was tested at two different relative densities ($D_r$): 30% and 80%. These are labelled in this paper as *loose* and *dense*

respectively. As will be shown later, these correspond to dry densities of 1·587 and 1·725 g/cm$^3$ respectively. These density limits were selected based on the in-situ density, measured using a nuclear gauge. The marl was tested at two different dry densities of 1·64 and 1·87 g/cm$^3$, corresponding to relative compactions (RC) of 81·4% and 92·8% respectively. For the marl, these conditions are labelled as *low density* and *high density* respectively. The marl samples were prepared with a water content equal to the optimum moisture content. The sabkha soil was tested at two different dry densities of 1·64 and 1·86 g/cm$^3$, corresponding to relative compactions of 85·2% and 96·8% respectively. For the sabkha, these conditions are labelled as *low density* and *high density* respectively. As the sabkha samples were collected from a location below the groundwater table, they were prepared with a water content equal to the optimum moisture content corresponding to the respective density from the compaction curve. Table 1 provides a summary of the properties of the tested soils.

The three soil types at the densities stated above were subjected to the following tests.

*5·2·1. Triaxial tests.* A set of at least four unconsolidated drained (UD) triaxial compression tests were conducted for each soil type at loose (low density) and dense (high density) conditions. These tests were done at confining pressures of 100, 200, 300 and 1000 kPa. Measurements included axial strain, deviator stress and volume change. The tests were performed according to ASTM Standards D 2850 and D 4767. They were performed at the very slow rate of loading of 0·0466 mm/min. Samples were loaded on the testing apparatus to a very high strain level, up to about 50%. Each test took about one day.

*5·2·2. Hydrostatic (isotropic) compression tests.* One test was conducted for each soil type at loose (low density) and dense (high density) conditions at confining pressures of 25, 50, 100, 200, 400 and 1200 kPa. The volume change and confining pressure were measured. This test is an isotropic compression test, which is similar to the triaxial test, but without applying any deviator stress, and with the confining pressure being increased in stages for each specimen. Each stage of confining pressure was maintained for about one day for the volume change to reach a stable value. The triaxial cell used for these tests was calibrated in order to indicate the cell expansion following the application of pressure. A solid steel cylinder with a volume equal to that of the soil sample was used in this calibration.

*5·2·3. Direct shear test.* A set of four direct shear tests were conducted for each soil type at loose and dense conditions. The vertical stresses applied were 100, 200, 300 and 1000 kPa. Measurements included vertical displacement, horizontal displacement and horizontal pressure. Tests were performed according to ASTM D 3080. Tests were made at the very slow rate of loading of 0·048 mm/min. For the marl and sabkha, the conventional apparatus was modified to allow for a large horizontal displacement, up to 26 mm instead of only 6 mm for the standard set-up.

## 6. RESULTS AND DISCUSSION

### 6.1. Physical properties

Particle size distribution (PSD) curves for all samples are shown in Fig. 3. The coefficients of uniformity, $C_u$, for the sand and marl are 1·744 and 3·285 respectively. The coefficients of curvature, $C_c$, for the sand and marl are 0·924 and 0·992 respectively. The sand was classified as *SP* (poorly graded sand) according to the Unified Soil Classification System, whereas the marl was classified as *SP* (gravelly sand with fines). The fine fraction of the marl was found to be non-plastic. For the sabkha, the 15% coarser than sieve # 200 was visually inspected and found to contain fine sand and remains of marine organisms. The clay fraction ($< 2\ \mu$m) was about 50%.

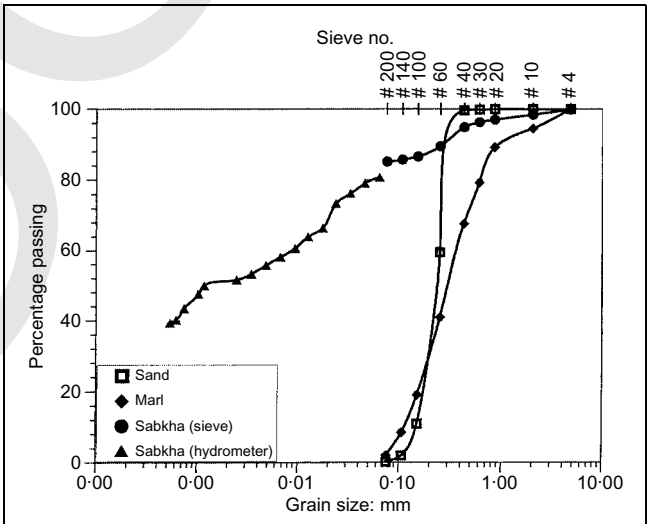


Fig. 3. Particle size distribution curve for the sand, marl and sabkha tested

| Soil | Unified classification | Condition | $D_r$: % | RC: % | $\rho_d$: g/cm$^3$ | $w$: % |
|---|---|---|---|---|---|---|
| Sand | SP | Low density | 30 | – | 1·587 | 0 |
| | | High density | 80 | – | 1·725 | 0 |
| Marl | SP | Low density | – | 81·4 | 1·64 | 9·1 |
| | | High density | – | 92·8 | 1·87 | 9·1 |
| Sabkha* | CL–ML | Low density | – | 85·2 | 1·64 | 23·25 |
| | | High density | – | 96·8 | 1·86 | 17·8 |

* Other properties include: PL = 22·9%, LL = 28·3%, PI = 5·4, $w_n$ = 25·6%.

Table 1. Soil properties

The specific gravity, $G_s$, of the sand, marl, and sabkha soils was 2·659, 2·639, and 2·853 respectively. The high sabkha value was attributed to the calcareous nature of these deposits, which may contain dolomite and calcium carbonate minerals that are known to have higher values for $G_s$.[26]

The natural water content, $w_n$, of the sabkha soil was

found to be 25·6%. The liquid limit (LL) and the plastic limit (PL) of the sabkha soil were found to be 28·3% and 22·9% respectively. The plasticity index (PI) was 5·4. This sabkha can be classified as *CL-ML* (silty clay).

The maximum and minimum densities ($\rho_{max}$ and $\rho_{min}$) obtained in the laboratory for the sand were found to be 1·787 and 1·515 g/cm$^3$ respectively. The in-situ density ($\rho_{field}$), as measured by the nuclear gauge, was found to be 1·641, 1·667, 1·690 and 1·712 g/cm$^3$ at depths of 5, 10, 20 and 30 cm respectively. The relative densities, $D_r$, of the loose and dense sands were 30% and 80%, respectively. Therefore the sand samples were prepared for loose and dense conditions at dry densities of 1·587 and 1·725 g/cm$^3$ respectively. These limits cover the range of in-situ results of the densities found in the field.

The compaction curve of the marl from the modified Proctor test (ASTM Standard D 1557) is shown in Fig. 4, which gives a maximum dry density ($\rho_{d,max}$) of 2·022 g/cm$^3$ and an optimum moisture content, $w_{opt}$, of 9·1%. Fig. 4 also shows the compaction curves of the sabkha from the modified Proctor test, which gave $\rho_{d,max}$ as 1·925 g/cm$^3$ and $w_{opt}$ as 13·55%. The optimum moisture contents for marl at low density ($\rho_d = 1{\cdot}64$ g/cm$^3$) and at high density ($\rho_d = 1{\cdot}86$ g/cm$^3$) are 23·25% and 17·8% respectively.

### 6.2. Results of triaxial tests

*6·2·1. Soil parameters.* This section presents the soil parameters obtained from triaxial tests performed on the various types of soil (sand, marl and sabkha) for both loose and dense conditions. The results of the triaxial tests are presented in terms of deviator stress, $\sigma_1 - \sigma_3$, against axial strain, $\varepsilon$, and volumetric strain against axial strain. The deviator stress at failure, $(\sigma_1 - \sigma_3)_f$, is taken as the value of deviator stress at the peak, provided that the peak occurs at a strain ($\varepsilon$) less than 15%. In the cases where the peak is not evident, or it occurs at $\varepsilon > 15\%$, the value of $(\sigma_1 - \sigma_3)_f$ is taken to be the value of the deviator stress at $\varepsilon = 15\%$, $(\sigma_1 - \sigma_3)_{\varepsilon=15\%}$, as suggested by Bowles.[27]

Figure 5 presents the results of triaxial tests on the low-density sand. Similar results were obtained for the high-density sand. The dense sand fails at a much lower strain and at a much higher deviator stress than loose sand. Also, the dense sand exhibits a smaller reduction in volume initially, and greater expansion at higher strain levels, compared with the loose sand. By increasing the confining pressure, the deviator stress increases and the volumetric strain decreases. This behaviour is similar to that reported in the literature.[28]

For the low-density sand ($D_r = 30\%$), and by using the Mohr–Coulomb failure criterion, the Mohr circles and the Coulomb failure envelope were drawn in Fig. 6. For this sand, the cohesion, $C$, was zero, and the angle of internal friction, $\phi_o$, was taken as the slope of the tangent of the first three circles, and found to be 38·30°. The reduction in the angle of internal friction, $\Delta\phi$, was taken to be the difference between the slope of the tangents of Mohr circles at confining pressures, $\sigma_3$, of 100 and 1000 kPa, and found to be 3·16°.

The parameters of the hyperbolic model were obtained from the triaxial data, according to the explanation given in section 2·1. Triaxial tests at $\sigma_3 = 100$, 200 and 300 kPa were considered in obtaining these parameters. The first step involves finding the initial tangent modulus, $E_i$, and the failure ratio, $R_f$, by plotting $\varepsilon/(\sigma_1 - \sigma_3)$ against $\varepsilon$, as defined earlier. Plots of $\varepsilon/(\sigma_1 - \sigma_3)$ against $\varepsilon$ are presented in Fig. 7 for the low-density sand. Fig. 7 represents a set of straight lines, each of which can be expressed by the equation of a straight line given in equation (3). The slope of each line gives $1/(\sigma_1 - \sigma_3)_u$ and

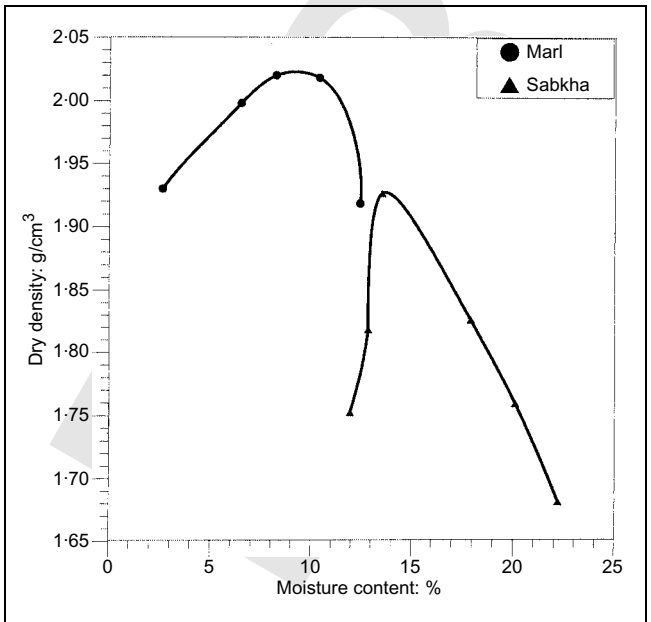


Fig. 4. Compaction curves for the marl and sabkha

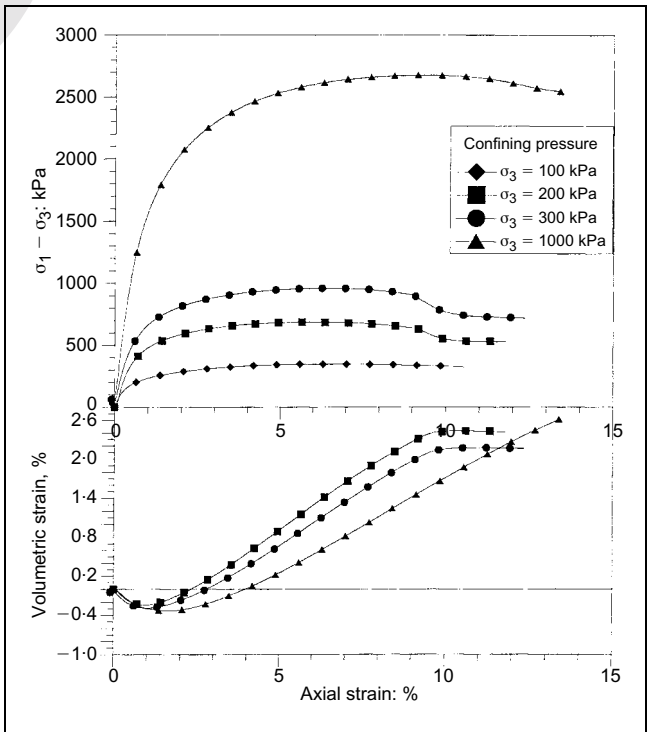


Fig. 5. Results of triaxial tests on the sand at low density

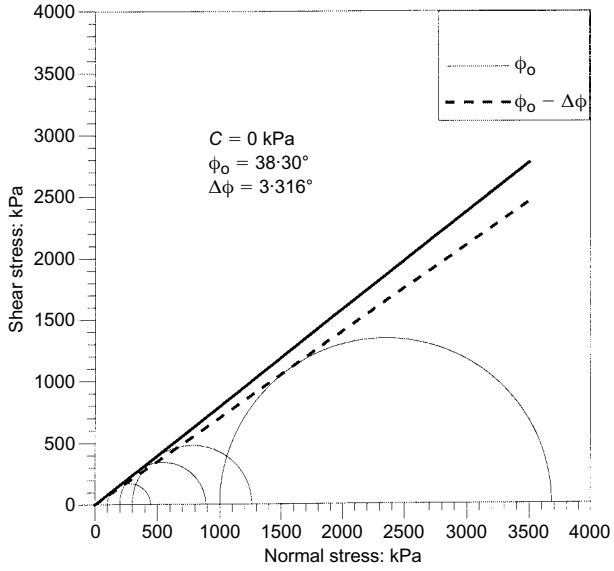


Fig. 6. Mohr circles for the sand at low density

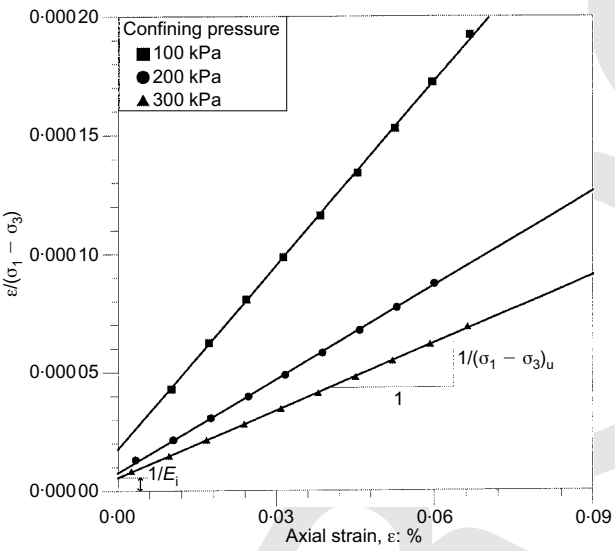


Fig. 7. Determination of $E_i$ and $R_f$ for sand at low density

the intercept gives $1/E_i$. Therefore $E_i$ is the reciprocal of the intercept, and $R_f$ is the slope times the peak value of the deviator stress, $(\sigma_1 - \sigma_3)_f$. Each line in Fig. 7 belongs to a specific confining pressure. For each confining pressure, the failure stress, $(\sigma_1 - \sigma_3)_f$, was obtained from Fig. 5, and the slope and the intercept were found from Fig. 7. The reciprocal of the slope gives $(\sigma_1 - \sigma_3)_u$, and the intercept equals $E_i$. Then the value of $R_f$ is calculated using equation (2). Table 2 provides the values for these parameters for sand at low density. The value of $R_f$ was found to be 0·897, 0·907 and 0·91 for $\sigma_3 = 100$, 200 and 300 kPa respectively, with an average value of 0·905.

The second step involves finding the parameters $K$ and $n$ of equation (4), by plotting the variation of $\log(E_i/P_a)$ against $\log(\sigma_3/P_a)$, where $P_a$ is the atmospheric pressure (Fig. 8). Equation (4) can be written as

$$\frac{E_i}{P_a} = K\left(\frac{\sigma_3}{P_a}\right)^n \quad (11)$$

or

$$\log_{10}\left(\frac{E_i}{P_a}\right) = \log_{10}(K) + n\log_{10}\left(\frac{\sigma_3}{P_a}\right) \quad (12)$$

Equation (12) represents the equation of a straight line in a log–log plot of $E_i/P_a$ against $\sigma_3/P_a$. The slope of this line is $n$, and the intercept at $\sigma_3/P_a = 1{\cdot}0$ is $K$. The values of $K$ and $n$ emerged as 585·89 and 1·07 respectively.

The above procedure was repeated for the high-density sand ($D_r = 80\%$), the marl at low and high density, and the sabkha at high density, and the values of the various parameters are given in Table 3. These parameters are comparable to those reported in the literature for similar soils.[12]

The results of triaxial tests on the marl at low and high densities are presented in Fig. 10. For the low-density marl, no increase in volumetric strain was experienced. For the high-density marl under a confining pressure of $\sigma_3 = 1000$ kPa the sample continued to experience a reduction in volume across the entire strain range. Triaxial test results for the marl at low and high densities were analysed following the procedure used for the sand.

The sabkha samples were prepared with water contents of 23·25% and 17·8% respectively, which correspond to those on the wet side of the optimum value from the compaction curve (Fig. 4). Triaxial test results for the high-density sabkha (RC = 96·8%) are presented in Fig. 11: these were analysed to determine the various parameters given in Table 3.

*6·2·2. Back-prediction.* The soil parameters obtained from triaxial tests on the various types of soil at different conditions (Table 2) were used to back-predict the stress–strain behaviour of these soils. The hyperbolic stress–strain relationships are given by equations (1)–(6). Substituting equations (2), (4), and (5) into equation (1) yields

$$\sigma_1 - \sigma_3 = \frac{\varepsilon}{\dfrac{1}{KP_a(\sigma_3/P_a)^n} + \dfrac{\varepsilon R_f(1-\sin\phi)}{2C\cos\phi + 2\sigma_3\sin\phi}} \quad (13)$$

where $\phi$ is given by equation (6). The predicted stress–strain curve for each soil type was then compared with the actual curves obtained from the experimental tests. Equation (13) is used for the back-prediction of the stress–strain relationship.

Figure 9(a) presents a comparison between the experimental and back-predicted stress–strain curves for the low-density sand, for $\sigma_3 = 100$, 200, 300 and 1000 kPa. The experimental and back-predicted curves are in very close agreement. Notice

| Confining pressure kPa | Peak stress, $(\sigma_1 - \sigma_3)_f$: kPa | Slope ($\times 10^{-3}$) | Intercept ($\times 10^{-6}$) | $(\sigma_1 - \sigma_3)_u = 1/$ slope ($\times 10^3$ kPa) | $E_i = 1/$intercept ($\times 10^5$ kPa) | $R_f = (\sigma_1 - \sigma_3)_f \times$ slope |
|---|---|---|---|---|---|---|
| 100 | 346·7 | 2·588 | 17·565 | 0·386 | 0·569 | 0·897 |
| 200 | 687·8 | 1·319 | 7·512 | 0·758 | 1·331 | 0·907 |
| 300 | 961·0 | 0·947 | 5·521 | 1·056 | 1·811 | 0·910 |

Table 2. Determination of $R_f$ from triaxial tests on sand at low density

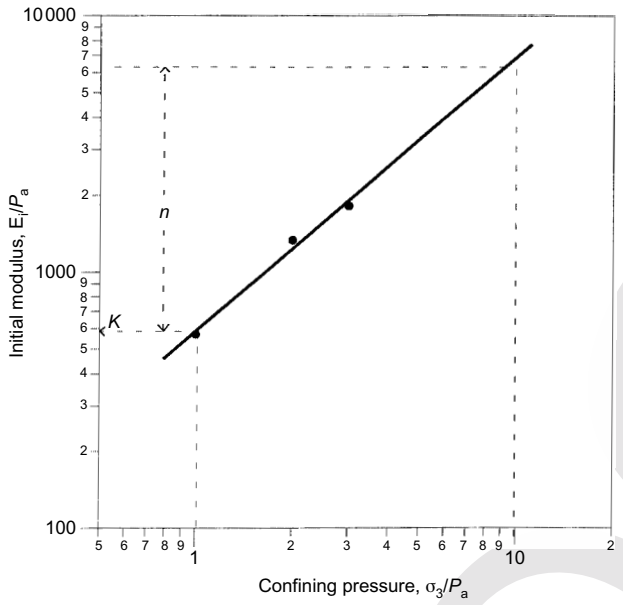


Fig. 8. Determination of model parameters $K$ and $n$ for sand at low density

that the soil parameters ($K$, $n$ and $R_f$) were determined based on the results of triaxial tests at $\sigma_3 = 100$, 200 and 300 kPa only; the experimental results for $\sigma_3 = 1000$ kPa were not included in the determination of these parameters. This was done to adhere to the standard procedure, and to avoid contaminating these parameters with non-linear effects at high confining pressure. Similar results were obtained for the high-density sand, as shown in Fig. 9(b). It is important to note that the hyperbolic model is not valid beyond the peak of the stress–strain diagram (point A, Fig. 1). This is because the hyperbola cannot capture the post-peak strain softening behaviour. In the case of soil materials exhibiting a sharp peak, such as dense soils, the peak usually indicates failure.

| Soil | $C$: kPa | $\phi_o$: deg | $\Delta\phi$: deg | $R_f$ | $K$ | $n$ |
|---|---|---|---|---|---|---|
| Sand (low density) | 0·00 | 38·31 | 3·32 | 0·90 | 585·89 | 1·07 |
| Sand (high density) | 0·00 | 46·40 | 3·47 | 0·85 | 1963·22 | 0·62 |
| Marl (low density) | 21·34 | 30·81 | 0·00 | 0·88 | 272·46 | 0·10 |
| Marl (high density) | 71·73 | 33·24 | 0·00 | 0·67 | 916·98 | 0·60 |
| Sabkha (high density) | 84·20 | 33·00 | 0·00 | 0·7 | 141·75 | 0·39 |

Table 3. Soil parameters obtained from triaxial tests

Figure 10 shows the experimental and back-predicted curves for the marl at low and high densities. The curves are in good agreement, especially up to the peak. Fig. 11 gives similar curves for the high-density sabkha soil.

### 6.3. Results of hydrostatic compression tests

*6·3·1. Soil parameters.* Soil parameters were obtained from hydrostatic (isotropic compression) tests performed on the various types of soil (sand, marl and sabkha) for both loose and dense conditions. The results of the hydrostatic compression tests for all three soil types are presented in Figs 12, 14, 15 and 16 in terms of confining pressure, $\sigma_m$, against volumetric strain, $\varepsilon_{vol}$. The volumetric strain was corrected to account for the expansion of the chamber upon applying the pressure. This expansion was considered as part of the calibration of the cells used for the hydrostatic compression tests.

Figure 12 presents the results of hydrostatic tests performed on the sand at low and high densities, in terms of hydrostatic stress, $\sigma_m$, against volumetric strain, $\varepsilon_{vol}$. The loose sand experienced more volumetric strain than the dense sand, especially at low values of hydrostatic stress. As the test progressed, the loose sand started to densify and the rate of reduction in volume reduced. The plot of $\sigma_m/\varepsilon_{vol}$ against $\sigma_m$ for the low-density sand is shown in Fig. 13. Equation (9) can be written as

$$\frac{\sigma_m}{\varepsilon_{vol}} = B_i + \frac{1}{\varepsilon_u}\sigma_m \quad (14)$$

Equation (14) is the equation of a straight line whose intercept represents the initial bulk modulus, $B_i$, and whose slope represents the reciprocal of the ultimate volumetric strain at large stress, $1/\varepsilon_u$. For the loose sand, the values for $B_i$ and $\varepsilon_u$ are 3,836·95 kPa and 0·0251 respectively.

The results of hydrostatic tests on the high-density sand, the marl and the sabkha were obtained and analysed, and the determined soil parameters are shown in Table 4. These parameters compare well with those reported by Selig[12] for similar soils. The hydrostatic tests were conducted on the

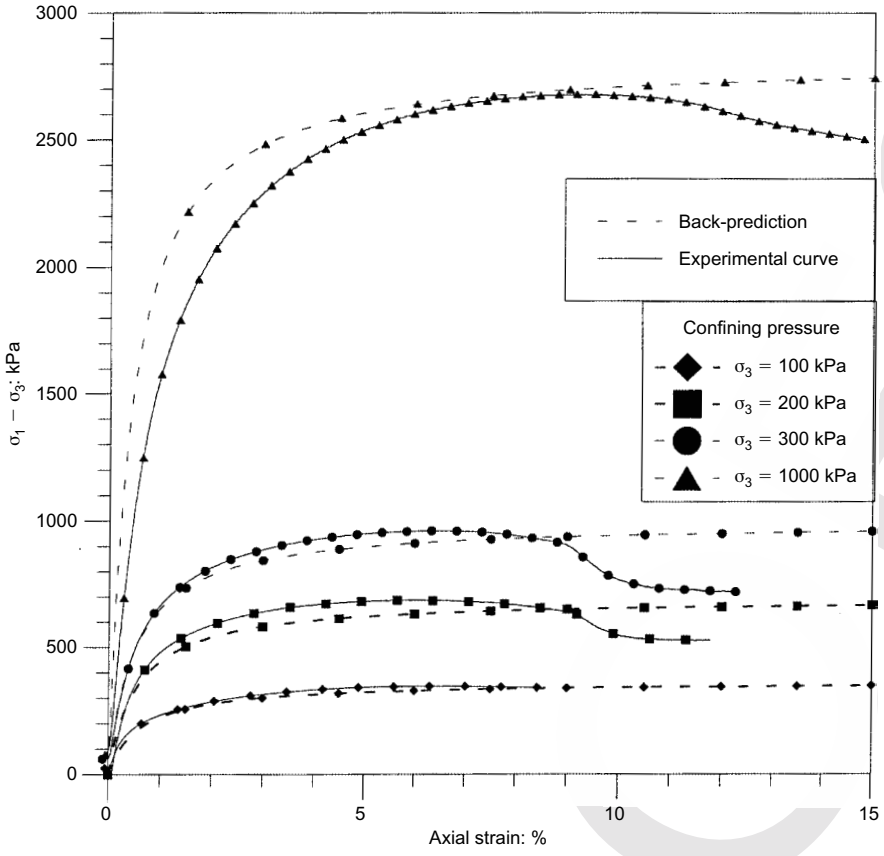


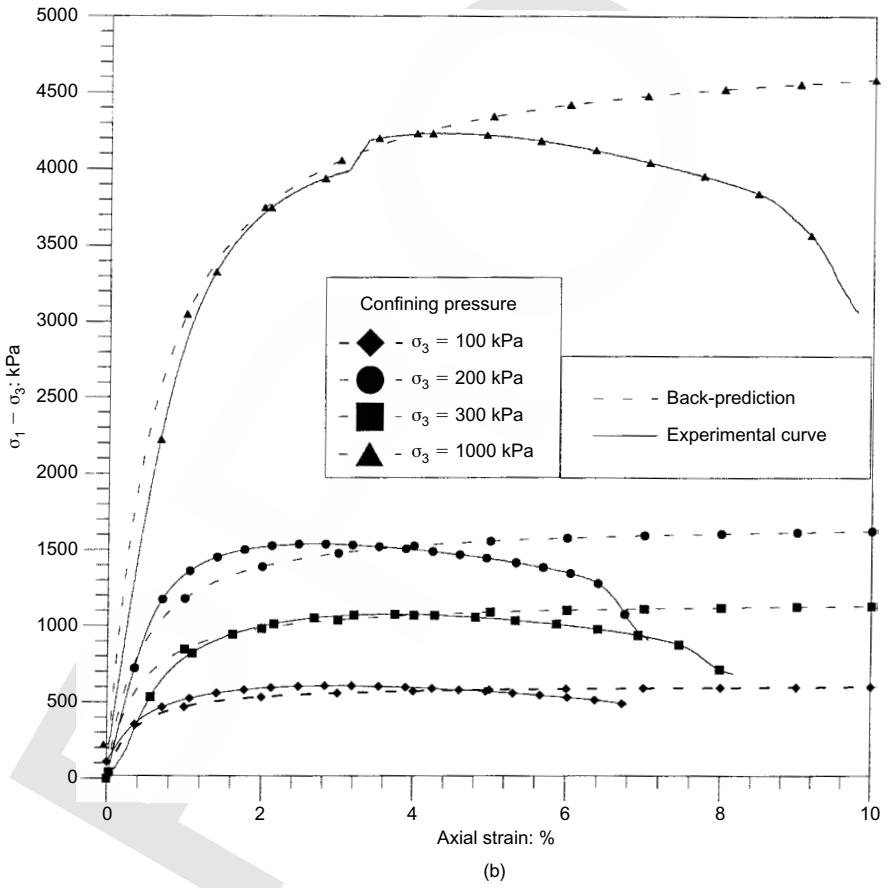


Fig. 9. Back-prediction of behaviour of sand under triaxial compression, at: (a) low density; (b) high density

sabkha at low and high densities, with water contents corresponding to the respective values of optimum water content. The low-density sabkha experienced more volumetric strain reduction than the high-density sample because of the amount of water lost during consolidation. Water was observed emerging from the sabkha soil samples during testing.

*6·3·2. Back-prediction.* The soil parameters obtained from hydrostatic tests on the various types of soil under different conditions (Table 4) were used to back-predict the behaviour of these soils under hydrostatic stress conditions. The predicted behaviour for each soil type is compared with the actual curve obtained from the experimental tests. The hyperbolic form, given in equation (9), was used to back-predict the behaviour of soils during hydrostatic loading.

Figure 14 presents comparisons between the experimental and back-predicted $\sigma_m$–$\varepsilon_{vol}$ curves for the low- and high-density sand. Similar results were obtained for the marl at low and high densities (Fig. 15), and for the sabkha (Fig. 16). The experimental and back-predicted curves are in very close agreement.

### 6.4. Results of direct shear tests

The results of the direct shear tests for all soil types are presented in terms of shear stress and normal displacement against horizontal displacement.

Figure 17 presents the results of direct shear tests on the low-density sand. Similar results were obtained and analysed for the high-density sand, the marl and the

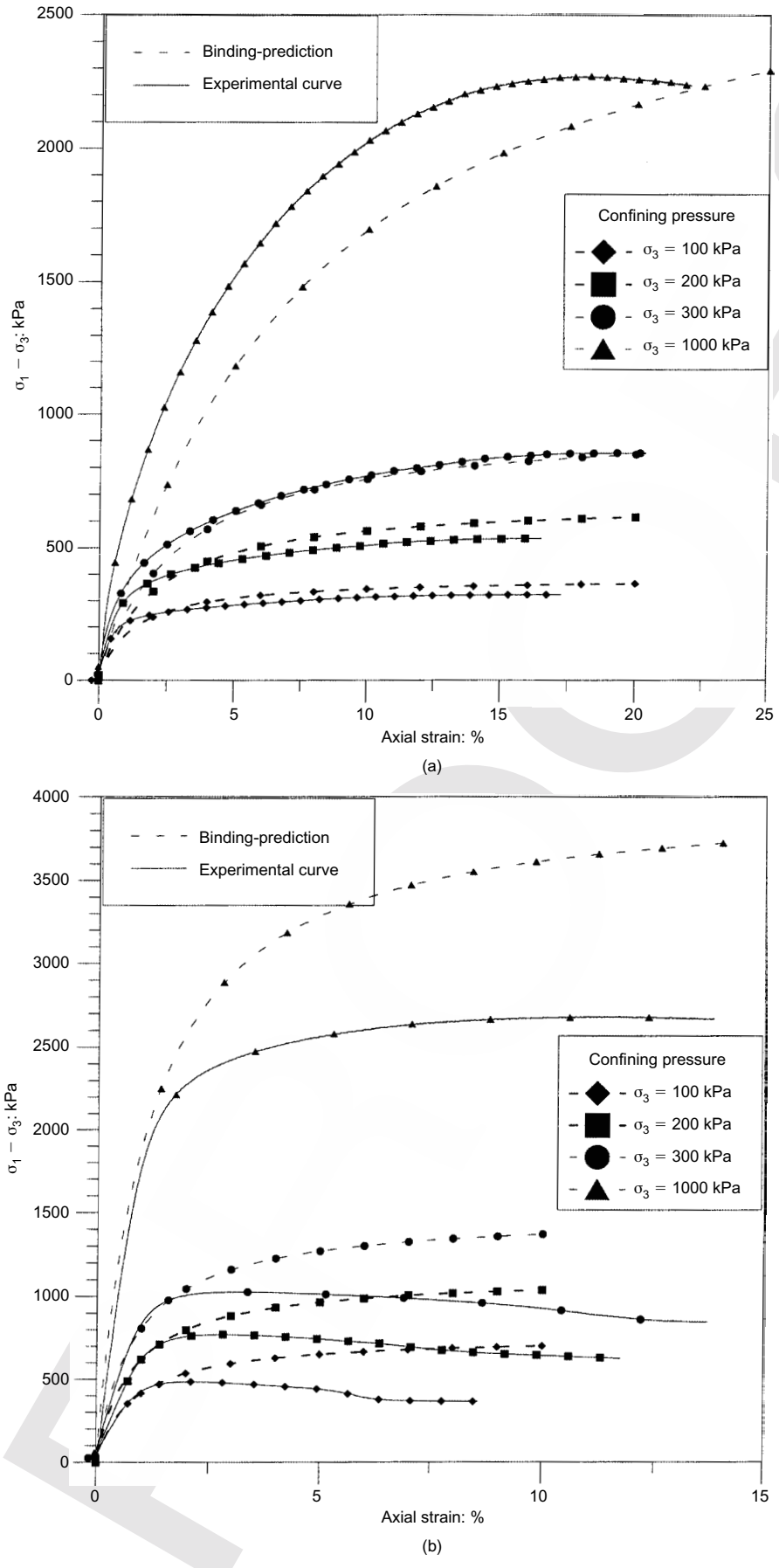


Fig. 10. Back-prediction of behaviour of marl under triaxial compression, at: (a) low density; (b) high density

sabkha (Table 5). The shear stress and the dilation (positive normal displacement) of dense sand are more, and the compression is less, than for loose sand. The shear stress, $\tau$, is taken as the value of $\tau$ at the peak of the shear stress–displacement curve, provided that peak occurs at a horizontal displacement of $\Delta H$ less than 6 mm (which corresponds to a shear strain of about 10%). In the cases where the peak in the shear stress–displacement curve is not evident, or where it occurs at $\Delta H > 6$ mm, the value of $\tau$ is taken to be that of $\Delta H = 6$ mm. The shear stress, $\tau$, of the loose sand is plotted against normal stress, $\sigma_n$, plotted in Fig. 18, from which $C = 0$, $\phi_o = 41{\cdot}4^\circ$ and $\Delta\phi = 2{\cdot}05^\circ$.

The results of direct shear tests on the marl at low and high densities showed an extremely large horizontal displacement, which exceeds the 6 mm limit for conventional results. The low-density marl did not experience any dilation, and its shear stress did not reach a peak value.

The results of direct shear tests were obtained for the sabkha soil at low and high densities, with water contents corresponding to the respective values of the optimum water contents. The low-density sabkha soil did not experience any dilation.

For all investigated soils, the cohesion ($C$) values obtained from direct shear tests are always less than those obtained from triaxial tests, and the values of the angle of internal friction ($\phi$) obtained from direct shear tests are always more than those obtained from triaxial tests. This is attributed to the restraining effect produced by the direct shear test box.

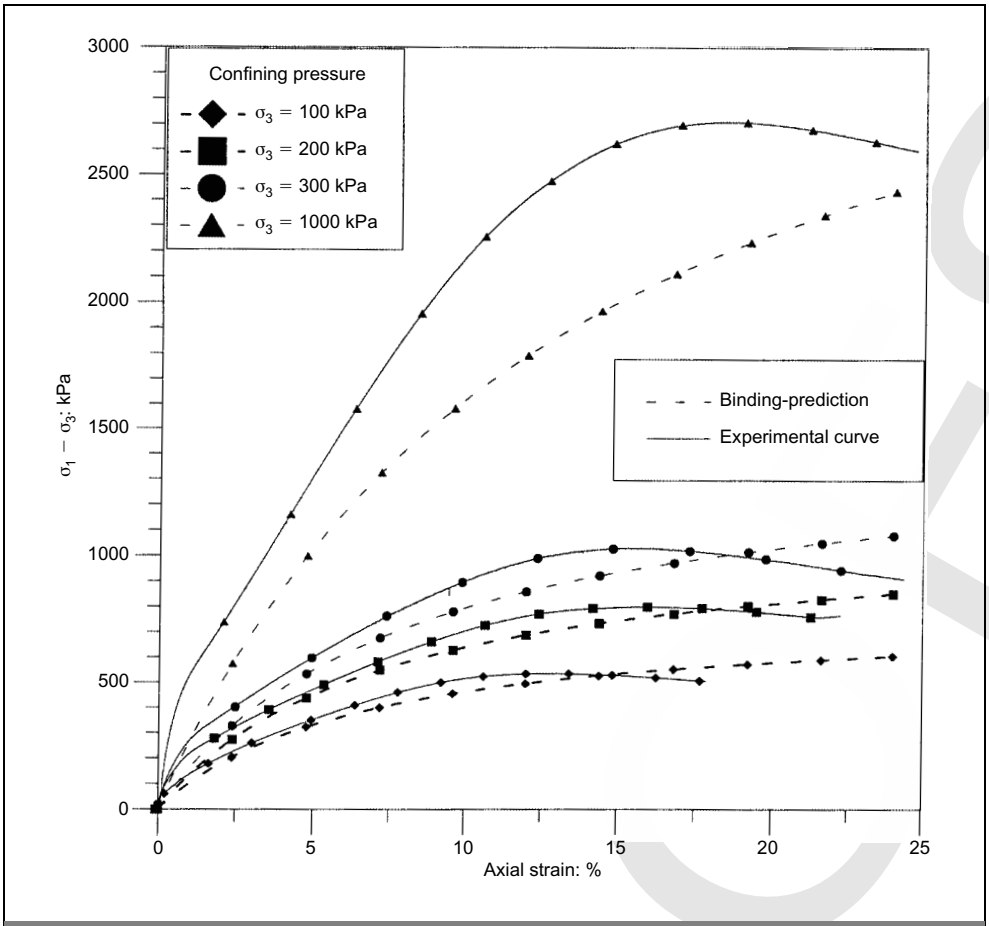


Fig. 11. Back-prediction of behaviour of sabkha under triaxial compression at high density

obtaining the parameters of these specific soils. These parameters were obtained for the three types of soil at different compaction levels, as shown in Tables 3 and 4. The values of these parameters are comparable to the range of values reported in the literature for similar soils. Using the obtained parameters, the models were found to successfully predict the experimental stress–strain response of the investigated soils under both triaxial compression and isotropic compression. Nevertheless, the parameters obtained belong specifically to the investigated soils and should not be generalised. Other soil materials require the determination of their parameters prior to using the hyperbolic model.

For the results from triaxial compression tests with a sharp peak of the stress–strain diagram, it is important

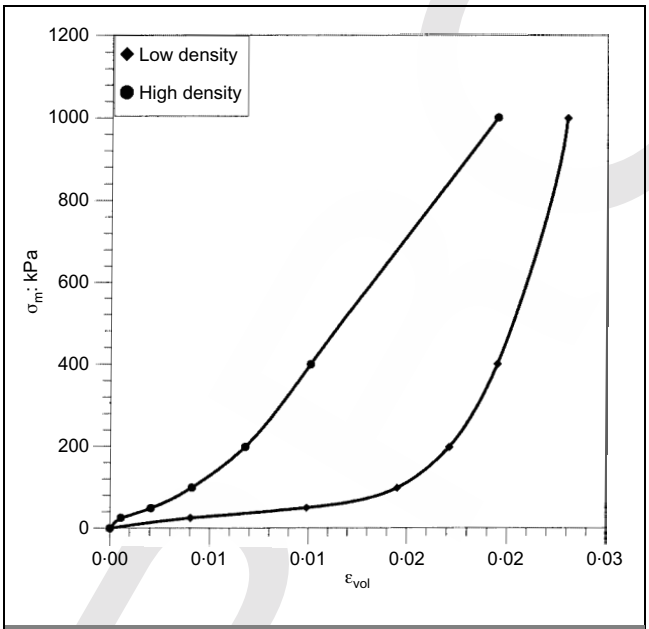


Fig. 12. Results of hydrostatic compression tests on sand

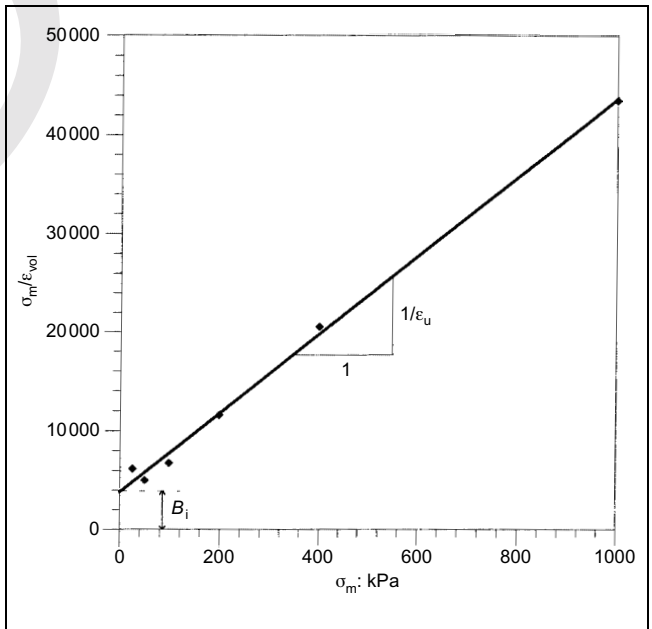


Fig. 13. Determination of $B_i$ and $\varepsilon_u$ for sand at low density

## 7. CONCLUSIONS

Three soil types from eastern Saudi Arabia were extensively characterised for the analysis of soil-interaction problems using the non-linear finite element method. The hyperbolic models for tangent Young's and bulk moduli were calibrated by

to note that the hyperbolic model is not valid beyond the peak. This is because the hyperbola cannot capture the post-peak strain softening behaviour. The peak value is considered to be the failure value, beyond which the soil sample is generally not of interest in non-linear elastic problems. For soil with a flat

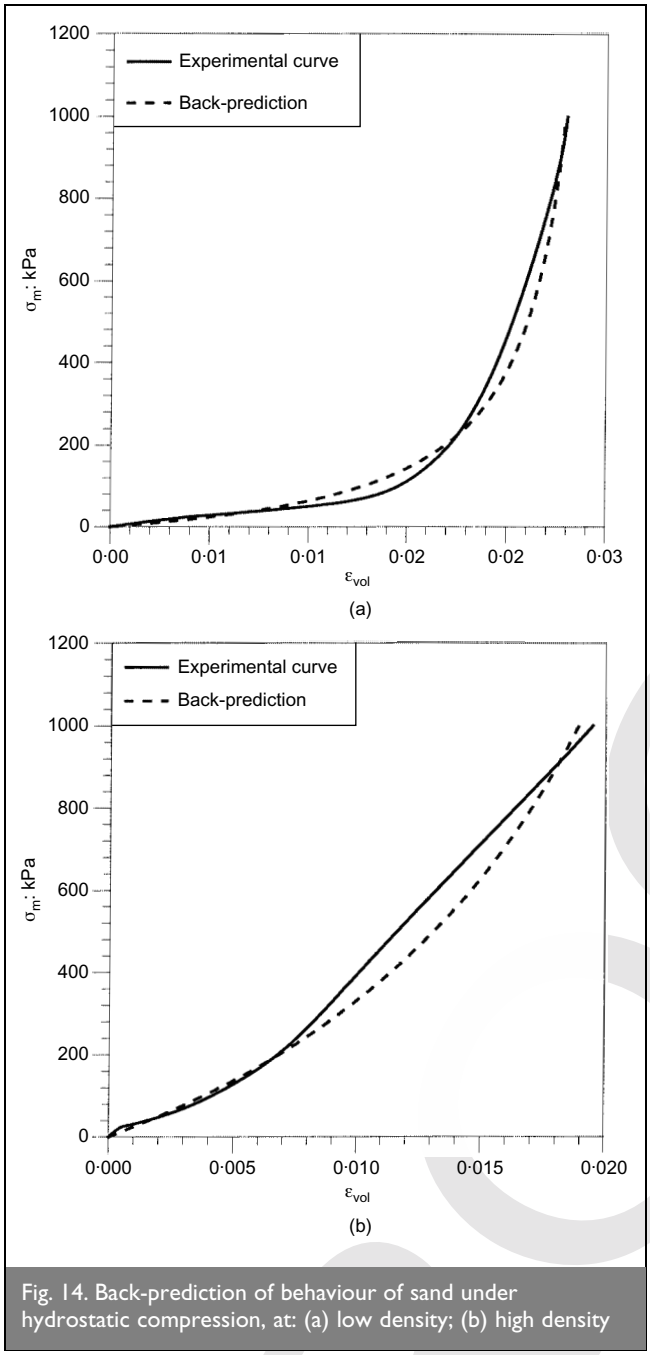


Fig. 14. Back-prediction of behaviour of sand under hydrostatic compression, at: (a) low density; (b) high density

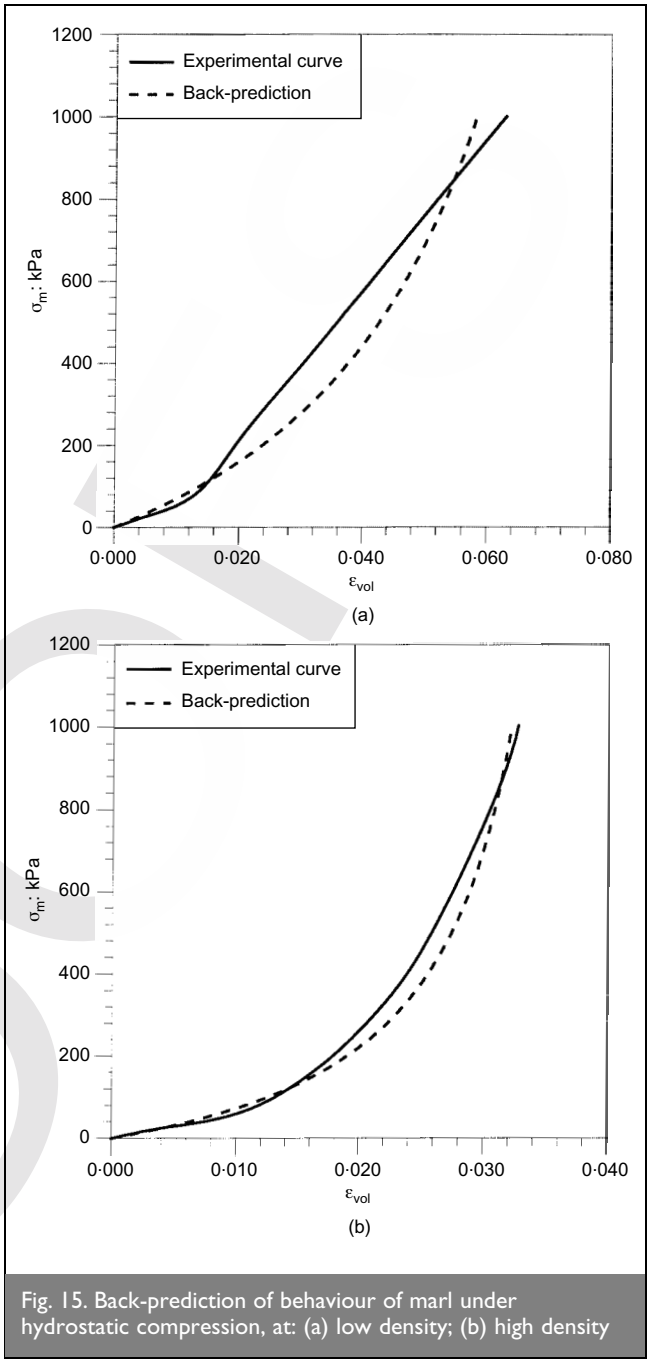


Fig. 15. Back-prediction of behaviour of marl under hydrostatic compression, at: (a) low density; (b) high density

| Soil | $B_i$: kPa | $\varepsilon_u$ | $B_i/P_a$ |
|---|---|---|---|
| Sand (low density) | 3 836·95 | 0·0251 | 38·37 |
| Sand (high density) | 23 275·90 | 0·0337 | 232·76 |
| Marl (low density) | 6 243·87 | 0·0915 | 62·44 |
| Marl (high density) | 5 356·65 | 0·0388 | 53·57 |
| Sabkha (low density) | 620·84 | 0·1420 | 6·21 |
| Sabkha (high density) | 2 608·77 | 0·0618 | 26·09 |

Table 4. Soil parameters obtained from hydrostatic tests

peak, the model can predict the soil behaviour up to extremely large strains. This shows the ability of this model to simulate excessive deformation of low-density soils.

At high confining pressure (1000 kPa), the triaxial results were predicted by the hyperbolic model with parameters obtained at relatively low confining pressure (100–300 kPa). This is considered to be another strength of this model, which can simulate the response of deep soil strata under high overburden pressure using results of conventional triaxial tests.

For hydrostatic (isotropic) compression, the hyperbolic model based on tangent bulk modulus shows strong capabilities to predict the behaviour of different soils.

## 8. ACKNOWLEDGEMENTS

The authors acknowledge the support of King Fahd University of Petroleum and Minerals in general, and the Civil Engineering Department and the Research Institute in particular, for providing computing, laboratory and editing facilities. They would also like to acknowledge Saudi-ARAMCO

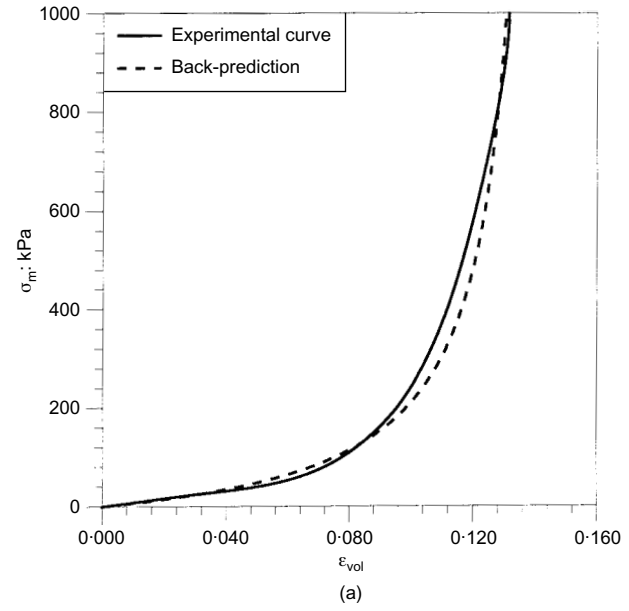


Fig. 16. Back-prediction of behaviour of sabkha under hydrostatic compression, at: (a) low density; (b) high density

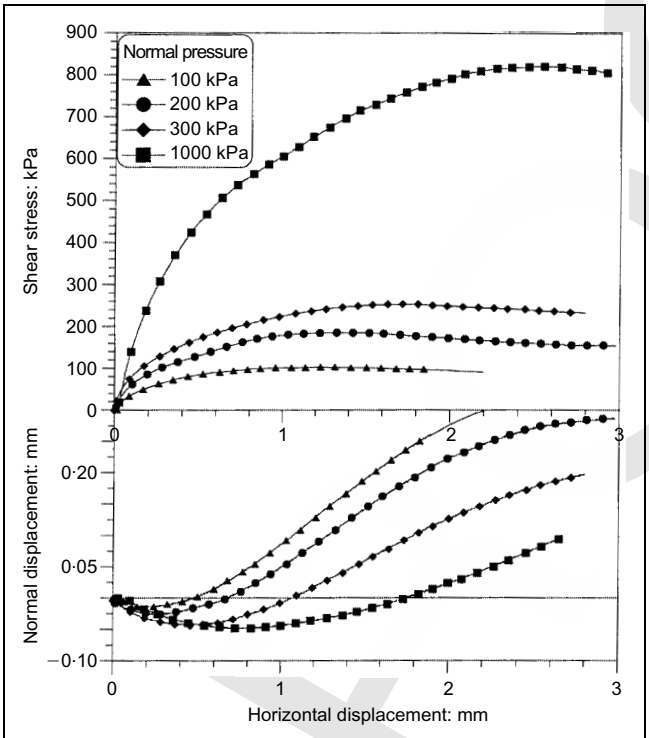


Fig. 17. Results of direct shear tests on low-density sand

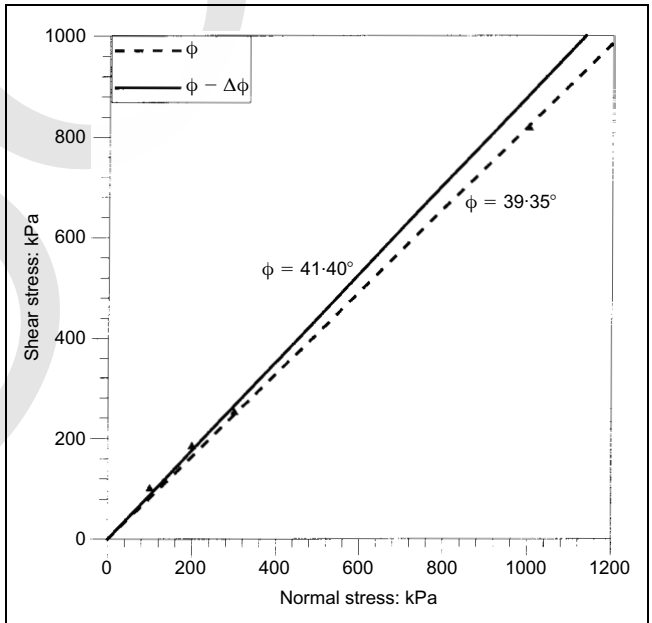


Fig. 18. Shear stress vs. normal stress for sand at low density

| Soil | $C$: kPa | $\phi_o$: deg | $\Delta\phi$: deg |
|---|---|---|---|
| Sand (low density) | 0·00 | 41·40 | 2·05 |
| Sand (high density) | 0·00 | 52·04 | 5·64 |
| Marl (low density) | 4·19 | 32·1 | 0·00 |
| Marl (high density) | 43·69 | 38·58 | 4·12 |
| Sabkha (low density) | 42·29 | 36·78 | 0·65 |
| Sabkha (high density) | 53·84 | 42·52 | 4·71 |

Table 5. Soil parameters obtained from direct shear tests

for supporting this research. Thanks also go to Mr Hasan Zakariya from the geotechnical laboratory.

## REFERENCES

1. COON M. D. and EVANS R. J. Recoverable deformation of cohesionless soils. *Journal of Soil Mechanics and Foundations Division, ASCE*, 1971, **97**, No. SM2, 375–391.
2. COROTIS R. B., FARZIN M. H. and KRIZEK R. J. Non-linear stress–strain formulation for soils. *Journal of the Geotechnical Engineering Division, ASCE*, 1974, **10**, No. GT9, 993–1008.
3. KO H.-Y. and MASSON R. M. Nonlinear characterization and analysis of sand. *Proceedings of the 2nd International Conference on Numerical Methods in Geomechanics*, 1976.

4. DESAI C. S. and SIRIWARDANE H. J. *Constitutive Laws for Engineering Materials, with Emphasis on Geologic Materials*. Prentice-Hall, Englewood Cliffs, NJ, 1984.
5. DUNCAN J. M. and CHANG C. Y. Nonlinear analysis of stress and strain in soils. *Journal of the Soil Mechanics and Foundations Division, ASCE*, 1970, **96**, No. SM5, 1629–1653.
6. WONG K. S. and DUNCAN J. M. *Hyperbolic Stress–Strain Parameters for Non-linear Finite Element Analyses of Stresses and Movements in Soil Masses*. Department of Civil Engineering, University of California, Berkeley, 1974, Report No. TE-74-3 to National Science Foundation.
7. KONDNER R. L. (1963), Hyperbolic stress–strain response: cohesive soils. *Journal of the Soil Mechanics and Foundations Division, ASCE*, 1963, **89**, No. SM1, 115–143.
8. KONDNER R. L. and ZELASKO J. S. A hyperbolic stress–strain formulation of sands. *Proceedings of the 2nd Pan-American Conference on Soil Mechanics and Foundation Engineering, Brazil*, 1963, **1**, 289.
9. HANSEN J. B. Discussion of 'Hyperbolic stress–strain response: cohesive soils' by R. L. Kondner. *Journal of the Soil Mechanics and Foundations Division, ASCE*, 1963, **89**, No. SM4, 241–242.
10. JANBU N. Soil compressibility as determined by oedometer and triaxial test. *Proceedings of the European Conference on Soil Mechanics and Foundation Engineering*, Wiesbaden, 1963, Vol. 1, pp. 19–25.
11. DUNCAN J. M., BYRNE P., WONG K. S. and MABRY P. *Strength, Stress–Strain and Bulk Modulus Parameters for Finite Element Analysis of Stresses and Movements in Soil Masses*. University of California, College of Engineering, Berkeley, CA, 1980, Report No. UCB/GT/80-01.
12. SELIG E. T. Soil parameters for design of buried pipelines. *Proceedings of the Pipeline Infrastructure Conference*, ASCE, 1988, pp. 99–116.
13. YANG G.-R. *Hyperbolic Young's Modulus Parameters for Compacted Soils*. Project Report ACP87-Pe for MS degree, University of Massachusetts, Amherst, MA, 1987.
14. LIN R.-S. D. *Direct Determination of Bulk Modulus of Partially Saturated Soils*. Project Report ACP87–341P for MS degree, University of Massachusetts, Amherst, MA, 1987.
15. POWERS L. F., RAMIREZ L. F., REDMOND C. D. and ELBERG E. L. Jr *Geology of the Arabian Peninsula: Sedimentary Geology of Saudi Arabia*. Arabian American Oil Company/United States Geological Survey (ARAMCO-USGS), 1963.
16. AL-SAYARI S. J. and ZÖTL J. G. *Quaternary Period in Saudi Arabia*, Vol. 1, Springer-Verlag, Wien, 1978.
17. ABDULJAUWAD S. N. Swelling behavior of calcareous clays from the Eastern Province of Saudi Arabia. *Quarterly Journal of Engineering Geology*, 1994, **27**, 333–351.
18. ABDULJAUWAD S. N. and AL-AMOUDI O. S. B. Geotechnical behaviour of saline sabkha soils. *Géotechnique*, 1995, **45**, No. 3, 425–445.
19. AZAM S., AL-ABDULJAUWAD S. N., AL-SHAYEA N. A. and AL-AMOUDI O. S. B. Expansive characteristics of gypsiferous/anhydritic soil formations. *Engineering Geology Journal*, 1998, **51**, No. 2, 89–107.
20. ABDULJAUWAD S. N., AL-SULAIMANI G. J., BASUNBUL I. A. and AL-BURAIM I. Laboratory and field studies of response of structures to heave of expansive clay. *Géotechnique*, 1998, **48**, No. 1, 103–121.
21. AL-SHAYEA N. A. Inherent heterogeneity of sediments in Dhahran, Saudi Arabia: a case study. *Engineering Geology Journal*, 2000, **56**, No. 3–4, 305–323.
22. AHMAD H. *Characterization and Stabilization of Eastern Saudi Marls*. MS thesis, Civil Engineering Department, King Fahd University of Petroleum & Minerals, Saudi Arabia, 1995.
23. AL-AYEDI E. S. *Chemical Stabilization of Al-Qurayyah Eastern Saudi Sabkha Soil*. MEng report, Civil Engineering Department, King Fahd University of Petroleum & Minerals, Saudi Arabia, 1996.
24. AL-GUNAIYAN K. A. *Assessment of the Geotechnical Properties of Sand-Marl Stabilized Mixtures for Constructional Purposes*. MS thesis, Civil Engineering Department, King Fahd University of Petroleum & Minerals, Saudi Arabia, 1999.
25. ASTM. *Annual Book of American Society for Testing and Materials (ASTM) Standards,* Vol. 04·08. ASTM, Philadelphia, PA, 1993.
26. LEE I. K., WHITE W. and INGLES O.G. *Geotechnical Engineering*. Pitman, Boston, MA, 1983.
27. BOWLES J. E. *Engineering Properties of Soils and Their Measurement*, 4th edn. McGraw-Hill, New York, 1992.
28. HOLTZ R. D. and KOVACS W. D. *An Introduction to Geotechnical Engineering*. Prentice Hall, Englewood Cliffs, NJ, 1981.

Please email, fax or post your discussion contributions to the secretary: email: mary.henderson@ice.org.uk; fax: +44 (0)20 7799 1325; or post to Mary Henderson, Journals Department, Institution of Civil Engineers, 1–7 Great George Street, London SW1P 3AA.

PROOF